REPORT DOCUMENTATION PAGE

Form Approved
OMB No. 0704-0188

1. REPORT DATE *(DD-MM-YYYY)*	2. REPORT TYPE	3. DATES COVERED *(From - To)*
02/23/2016	Final Technical	JAN 2011 - DEC 2013

4. TITLE AND SUBTITLE
Power-Scalable Blue-Green Bessel Beams

5a. CONTRACT NUMBER

5b. GRANT NUMBER
N00014-11-1-0098

5c. PROGRAM ELEMENT NUMBER

6. AUTHOR(S)
Siddharth Ramachandran

5d. PROJECT NUMBER

5e. TASK NUMBER

5f. WORK UNIT NUMBER

7. PERFORMING ORGANIZATION NAME(S) AND ADDRESS(ES)
Boston University
Office of Sponsored Programs
25 Buick St.
Boston, MA 02215

8. PERFORMING ORGANIZATION REPORT NUMBER

9. SPONSORING/MONITORING AGENCY NAME(S) AND ADDRESS(ES)
Michael Wardlaw
Office of Naval Research
875 North Randolph St.
Arlington, VA 22203

10. SPONSOR/MONITOR'S ACRONYM(S)

11. SPONSOR/MONITOR'S REPORT NUMBER(S)

12. DISTRIBUTION/AVAILABILITY STATEMENT
Approved for Public Release; distribution is unlimited

13. SUPPLEMENTARY NOTES

14. ABSTRACT
See attachment.

15. SUBJECT TERMS
intermodal nonlinearities, high-power all-fiber lasers, non-traditional emission wavelengths, high-power blue-green tunabel lasers

16. SECURITY CLASSIFICATION OF:			17. LIMITATION OF ABSTRACT	18. NUMBER OF PAGES	19a. NAME OF RESPONSIBLE PERSON
a. REPORT	b. ABSTRACT	c. THIS PAGE			Siddharth Ramachandran
					19b. TELEPHONE NUMBER *(Include area code)*
U	U	U	SAR	11	617-353-9811

Power-Scalable Blue-Green Bessel Beams

Siddharth Ramachandran
Photonics Center, Boston University, 8 Saint Mary's Street, Boston, MA 02215
phone: (617) 353-9881 fax: (617) 353-6440 email: sidr@bu.edu

Award Number: N00014-11-1-0098
http://people.bu.edu/sidr

ABSTRACT

The overall goal of this program was to demonstrate intermodal nonlinearities as a pathway for high-power all-fiber lasers at non-traditional emission wavelengths, and then to demonstrate a proof of concept of this methodology for achiveing high-power blue-green tunabel lasers. The first part of the program, namely demonstrating that the use of Bessel beam like high order optical modes for nonlinear frequency translation, and hence emission, at non-standard wavelengths was highly successful, and cascaded emission down to 453 nm was achieved. We showed that a simple double-clad fiber suffices for all these demonstrations, thereby enabling significant cost reductions for future systems that employ this technique. We also showed that this technique is eminently scalable, and achieved tunable lasers in the 1um range with > 10 kW of peak power. The second part of the program, namely specifically building system to achieve emission at the *desired* blue colours, was, however, abandoned due to lack of funds relative to the original anticipated award amount.

Power-Scalable Blue-Green Bessel Beams

Siddharth Ramachandran
Photonics Center, Boston University, 8 Saint Mary's Street, Boston, MA 02215
phone: (617) 353-9881 fax: (617) 353-6440 email: sidr@bu.edu

Award Number: N00014-11-1-0098
http://people.bu.edu/sidr

LONG-TERM GOALS

Underwater and air-water light-based sensing systems would critically benefit from sources that can emit optical pulses with high enough energy to withstand losses due to turbulence and scintillation, both, in low visibility air, as well as underwater. An attractive schematic would be to use high energy pulsed lasers.

This scheme would be operationally effective only if the lasers and sources could be mounted on a variety of different platforms, ranging from aircraft and ships, to submarines, as Fig. 1a illustrates. This, in turn, means that the lasers must be robust, portable, compact, *and* must possess high wall-plug efficiencies. An additional constraint is dictated by the Jerlov chart, shown in Fig. 1b, which indicates that such sources must be within the blue-green spectral range in order minimise losses in ocean waters. Ideally, one would benefit from a source that can be designed to span this wavelength range so as to deploy this capability at any desired ocean depth.

(a) (b)

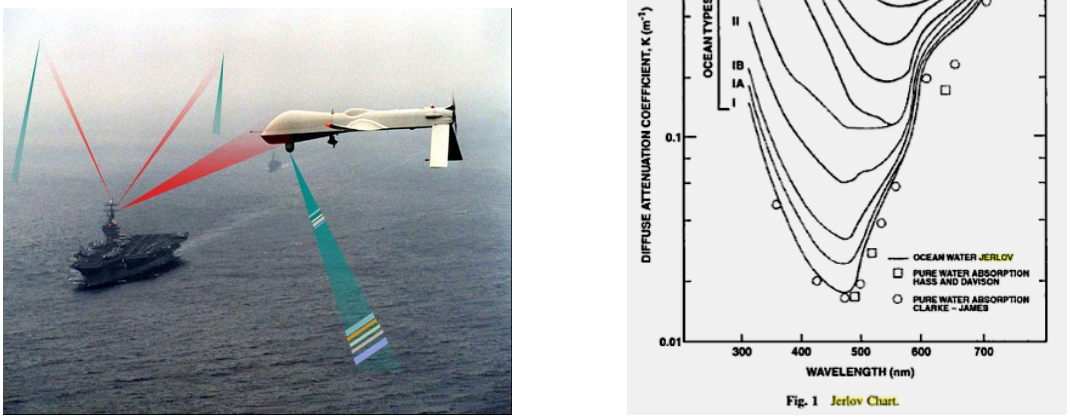

Fig. 1: (a) Schematic of a versatile air-to-sea communications as well as a submarine communications link, illustrating an integrated capability of high-bandwidth communications between multiple naval points of interest. (b) Jerlov chart showing the transmission spectral loss minima at different depths of ocean water.

OBJECTIVES

Satisfying all these demanding requirements has led to tremendous interest in, and efforts towards, developing blue-green laser sources that could enable such sensing systems. One potential approach is to develop compact, efficient, mJ-level pulsed sources, and then to externally modulate them. Unfortunately, even this power level is difficult to achieve without using traditional gas or solid state sources that are simply too bulky, power inefficient for practical deployment on naval vehicles, especially aircraft. Fiber lasers have been proposed as an alternative, but while they are light and compact, nonlinear distortions in such lasers have traditionally limited scalability to the ~1 mJ range. This is especially true in the case of attempting blue-green lasers with them, since they need to be frequency doubled, which further decreases power levels. More debilitating is the fact that modulating them requires the ability to externally modulate the 1060 nm (Yb:fiber) or 4xx-5xx nm (frequency doubled) laser, and this technology is simply not as advanced as that in the telecom spectral range.

APPROACH

The schematic of the proposed device is shown in Fig. 2. Two commercial Yb:doped fiber laser operating at 103x and 106x nm are combined with a WDM, and fiber I generates a near-IR photon around 760 nm. This output is fed to a different fiber II, which generates the desired blue-green photon. The percentage value at each point in the schematic refers to efficiency of that specific process. Overall, starting with X mJ of energy from fiber lasers in the 10xx nm range, one obtains 1.4 X mJ of near-IR photons or 1.2 X mJ of blue/green photons. In comparison, the conventional approach of using a powerful 10xx nm fiber laser and frequency-doubling its output yields only ~ 0.5-0.6 X.

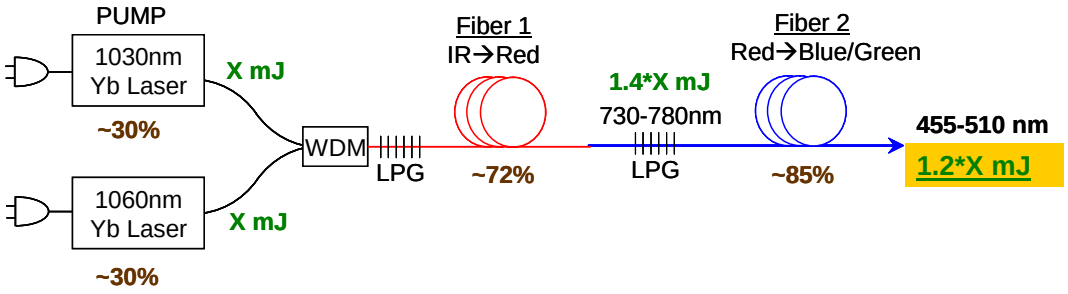

Fig. 2: Schematic of monolithic fiber laser producing blue-green pulses. Commercially available 10xx nm lasers are multiplexed in a tree architecture into two fibers of type I, whose near-IR output is again multiplexed to achieve blue. Conversion efficiencies: IR-> near-IR ~ 72% and near-IR -> blue/green, 85%, yielding (with typical wall-plug efficiencies of 10xx nm lasers of 25-30%) overall efficiency of ~18%.

The device architecture relies on a 10xx nm fiber laser platform that is not only well developed, but is continually improving due to engineering enhancements related to thermal and nonlinear management. Thus, the power of the blue-green output out of our device will directly scale with the power of commercial 1060-nm fiber lasers. Most importantly, our architecture presents the unique possibility of achieving in-fiber coherent combination of lasers – the obvious benefit of this approach is the ability to combine beam combination, of necessity to scaling power, with the compactness and robustness of an all-fiber device.

The critical building block that enables this architecture is the ability to achieve four wave mixing between different modes in a fiber. Specifically, the two four-wave mixing fibers must have phase matching curves, as shown in Fig. 3, that enable coherent conversion of photons from 10xx nm to the blue-green spectral range.

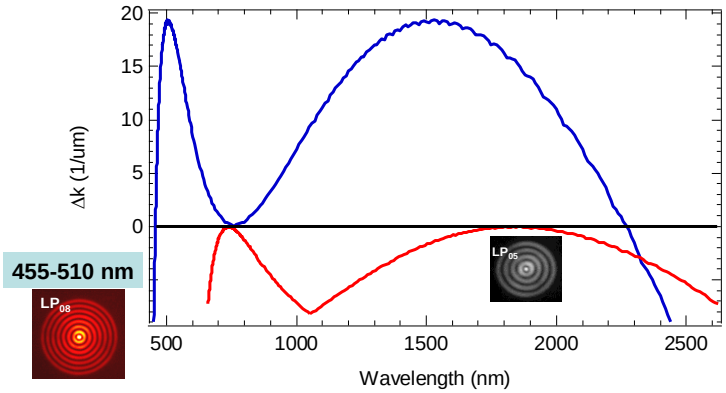

Fig. 3: Phase matching curve (Δk) for fiber I (red) and fiber II (blue). Fiber I multiplexes two 10xx nm pulses to yield a near-IR and mid-IR pulse (with most energy in the near-IR pulse), and fiber II repeats this process to yield desired blue-green photons.

Key Personnel:

Prof. Siddharth Ramachandran, PI (US Permanent Resident)
3 Graduate students (Lu Yan, Yuhao Chen and Jeff Demas), one Visiting researcher (Lars Rishoj), one post-doctoral associate (Paul Steinvurzel) and one undergraduate student (Zhiji Liu).

WORK COMPLETED

Following successful completion of CY 2011 and CY 2012 tasks, the project ccompleted the critical task for CY 3 (project start date was Jan. 1, 2011 and not the beginning of FY-2011) – namely, the demonstration of parametric nonlinear wavelength conversion at high energy levels in optical fibers. Progress towards program goals are succintly depicted in the Gannt chart below (Fig. 4). With respect to overall program goals, the final task, of cascaded power combining of pulses, was not executed, and the intermediate task, of power combining with HOMs, was terminated due to a shortfall of received funds relative to the proposed effort, hence bringing the program to a halt. The tasks executed are shown with a white tick mark, and thoe abandoned as decribed above, are shown with a red cross.

Task	CY 2011 1st Half	CY 2011 2nd Half	CY 2012 1st Half	CY2012 2nd Half	CY2013 1st Half	CY2013 2nd Half
Theory & Design (fiber design + parametric sim)	✓					
Fabricate fiber 1	✓	✓				
Fabricate/assemble Gratings & Devices	✓	✓	✓			
Seed/pump laser assembly		✓	✓	✓	✓	✓
HOM Parametric Demo		✓	✓			
Fabricate fiber II + gratings		✓	✓	✓		
Cascaded HOM Parametric to Blue			x	✓		
Iterate design & fabricate fiber & gratings			✓	✓	✓	
Power combining with HOMs				✓	X	
Iterate design & fabricate fiber & gratings				✓	✓	✓
Cascaded Power Combining to Blue					X	X

Fig. 4: Gantt chart showing overall program goals and progress towards them, with tick marks for tasks completed.

RESULTS

A summary of the results achieved is given in the following bulleted list:

➢ **Fiber Characterization:** Device fabrication in the newly obtained fibers from Nufern posed both a challenge as well as opportunity to utilize the considerable device fabrication experience we gained in the first year of the program while creating Bessel beams. Figure 5 shows (a) the fiber design provided to Nufern, in comparison to (b) the profile of the fabricated fiber. Note that large index dip in the center, which led to the fundamental mode beam quality being as bad as $M^2 > 2$. This led to two operational problems – input coupling from a laser was high loss *and* it created a large amount of intermodal interference making the task of mode-converting to the desired HOM almost impossible.

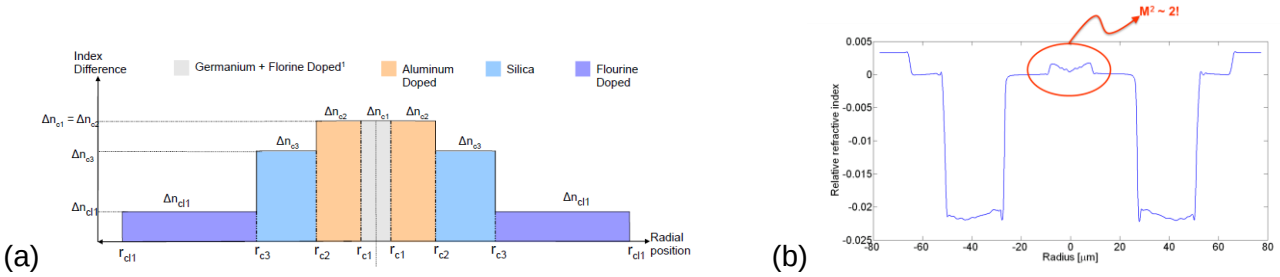

Fig. 5: (a) Fiber design sent to Nufern, and (b) index profile of fiber obtained from Nufern – note the large deviation in the center of the profile.

➢ **Device Fabrication:** We solved this problem by applying innovative mode-stripping techniques to ensure that, even though the input into this fiber excited all the modes of the fiber, the output was pure and mono-moded. This is schematicaly illustrated in Fig. 6, which shows the dramatic difference between the modes excited in the as-fabricated fiber and the modes in the fiber that have a taper-etch based mode stripper (the taper-etch functions only when index matched with oil, and hence the effect of the device is easy to deduce by measuring device performance before and after the introduction of oil. Thus, we demonstrate strong, pure mode conversion to the desired modes.

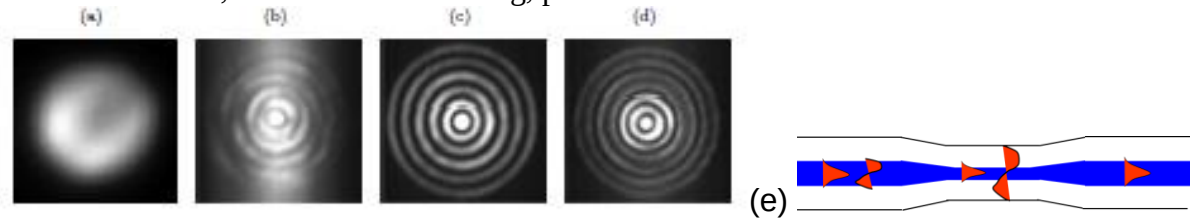

Fig. 6: (a) Fundamental mode in the 130 μm OD fiber. (b) At resonance wavelength in the LP_{06} grating, before adding oil to the tapered etched region. (c) At resonance wavelength in the LP_{06} grating, after adding oil to the tapered etched region. (d) At resonance wavelength in the LP07 grating, after adding oil to the tapered etched region; (e) Schametic of tapered-etched device that performs the mode-stripping function.

➢ **Bottle beams demonstration with all fiber tuning**: In this work, we demonstrate optical bottle generation from selective excitation of two Bessel-like $LP_{0,m}$ fiber modes, a geometry which is directly analogous to double-axicon or double annular slit experiments. This is experimentally realized by cascading two long period gratings (LPGs). Our method enables us to independently tune the relative amplitudes and phases of the interference terms, so that we can dynamically control both the depth and location of the bottles. This enables a high degree of control of the beam, available otherwise only from Spatial Light Modulators (SLM). Additionally, fibers allow alignment-free remote delivery of the beam.

A schematic of the experiment is shown in Fig. 7(a). We UV write two 1 cm long gratings, separated by 5 cm, in a high NA single mode fiber (SMBD0980B, OFS). The first grating has a pitch of 100.6 μm and

couples to the $LP_{0,5}$ mode, whereas the second has a pitch of 435 μm and couples to the $LP_{0,15}$ mode. The gratings are characterized individually by placing index matching gel on one and measuring the spectral response of the other. The respective spectra are shown in Fig. 7(b). We couple light from an external cavity laser (ECL) (HP 8168F) tuned to 1563 nm, image the cleaved end facet on an InGaAs CCD camera (NIR300, Vosskühler GmbH) with a 60× objective lens, and record a 3-D image stack as we move the lens and camera longitudinally away from the fiber facet. At the excitation wavelength of 1563nm, we couple 28% of the power into the $LP_{0,5}$ mode and 72% of the power to the $LP_{0,15}$ mode The y-cut of the measured tomogram and a 2-D image of the bottle at z = 216 μm are shown in Figs. 7(c) and (d).

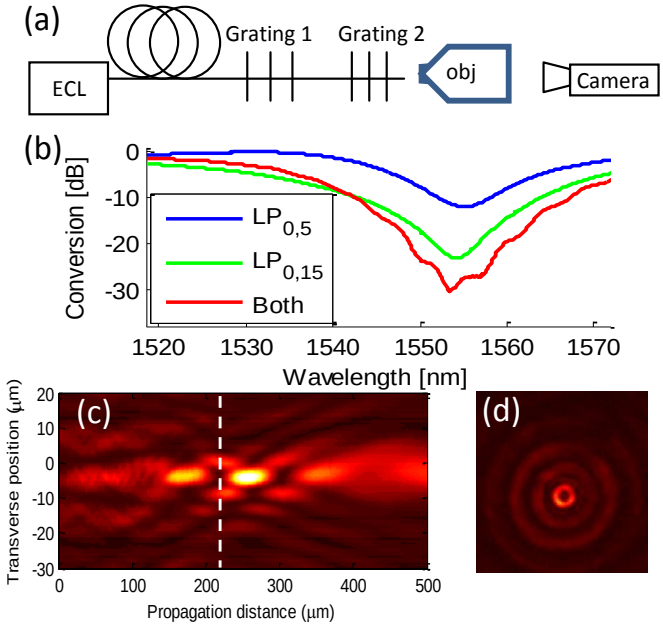

Fig.7: (a) Experimental setup (b) LPG spectra of grating 1 ($LP_{0,5}$), grating 2 ($LP_{0,15}$), and both gratings. (c) A tomogram of the y-axis cut. (d) 2-D cross-section of the bottle at z=216 μm (dashed line).

➢ **High power four wave mixing demonstrations:** For the experiment, we designed a concentric core fiber, manufactured by Nufern, Inc. In Fig. 8(a) we show an end facet microscope image of the fiber, indicating the outer core where the HOM is guided, and the inner core which controls the modal content of the input coupling, described below. We use the measured refractive index profile of the fiber, shown in Fig. 8(b), to simulate the $LP_{0,m}$ modes and calculate their GVD and A_{eff}, plotted in in Figs. 8(c) and (d). As the radial mode order increases, the zero dispersion wavelength shifts blue [9], though A_{eff} is not strongly affected by mode order (the $LP_{0,1}$-$LP_{0,3}$ modes are not plotted because the inner core does affect their GVD and A_{eff}, so they are inappropriate for the GVD engineering described here). One can design a fiber to handle a particular power level by first choosing the outer core diameter, which roughly scales with A_{eff}. Then, find the mode that has the right amount of anomalous GVD at a desired wavelength, and thus providing parametric gain at that wavelength. In the present case, the $LP_{0,7}$ mode (shown by the bold black lines in Fig. 8) has weakly anomalous GVD = +5.4 ps/nm/km and A_{eff} = 614 μm^2 at 1.064 μm, our chosen pump wavelength.

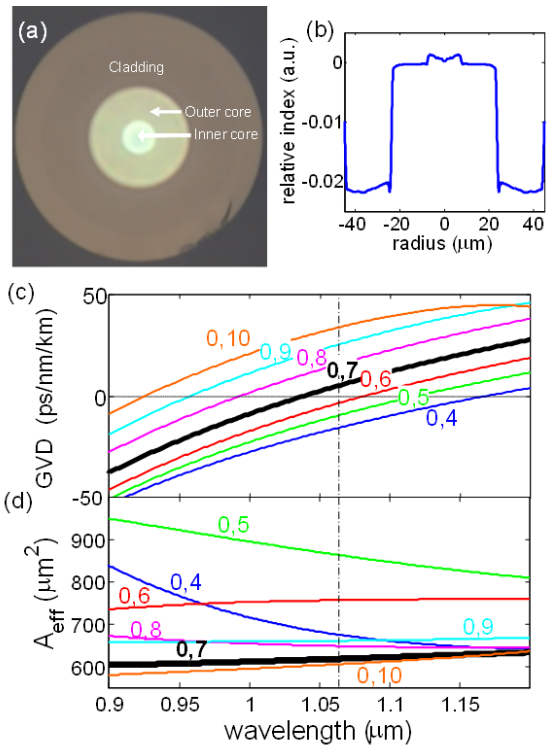

Fig. 8 (Color online) (a) Microscope image of the custom HOM fiber end facet. (b) Experimentally measured refractive index profile of the fiber, plotted relative to the index of silica. (c) Dispersion and (d) A_{eff} of $LP_{0,m}$ modes of a custom HOM fiber as a function of radial mode order. The bolded lines indicate the $LP_{0,7}$ mode used in this work, vertical dashed line indicates the pump wavelength at 1.064 μm

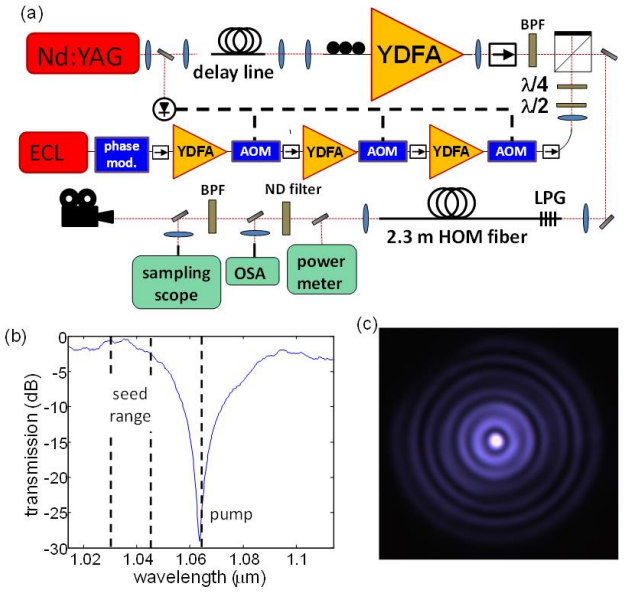

Fig. 9 (Color online) (a) Schematic diagram of the HOM PWC experiment. (b) Transmission spectrum of the LPG mode converter, with the pump and signal seed wavelengths indicated. (c) Measured image of the $LP_{0,7}$ mode at 1.064 μm.

A schematic of the experiment is shown in Fig. 9(a). The pump is a Q-switched Nd:YAG microchip laser (Teem photonics SNP-20F) with a 0.5 ns pulse width and 19.56 kHz rep. rate amplified in a large mode area (LMA) Ytterbium doped fiber amplifer (YDFA) to a peak power of ~87 kW. A bandpass filter (BPF) with 4 nm 3-dB bandwidth (Semrock LL01-1064) at the pump output cleans up the pump spectrum. We found that the temporal shape of the pump pulse depended on the setting of the polarization controller at the YDFA input. For some settings, we obtained a smooth, Q-switched pulse similar to the microchip laser output, but for other settings, which yielded stronger spontaneous MI at the HOM sample output, the temporal profile exhibited some intensity modulation which may arise from polarization mode beating.

The repetition rate of the Nd:YAG laser is stable only to 1-2%, so we tap off part of that beam to a photodetector which we use to trigger the acousto-optic modulators (AOMs) in the multi-stage YDFA which serves as the anti-Stokes seed. In order to synchronize the arrival of the pump and seed pulses at the sample input, we delay the pump pulse through 100 m of passive LMA fiber (Nufern LMA-GDF-20/400-M) before amplification. The anti-Stokes seed is a wavelength tunable low power external cavity laser (ECL) temporally modulated and amplified in three single mode YDFA stages to a peak power of 100-200 W. A phase modulator broadens the ECL linewidth to 1.7 GHz to suppress SBS in the first stage, and AOMs between the stages chop the seed into 8 ns pulses.

The pump and seed are combined with a beamsplitter and focused into the 2.3 m HOM fiber sample coiled with a bend radius of 15 cm. We focus the beams into the Ge-doped inner core to excite the $LP_{0,1}$ mode and then convert it to $LP_{0,7}$ mode of the outer core using a UV-written long period grating (LPG) coupler [11]. The LPG is located 5 cm from the input facet, and the $LP_{0,1}$ mode has an A_{eff} of 264 μm^2, so we do not anticipate any nonlinearities to arise before the mode converter. The LPG transmission spectrum, measured by butt-coupling

the fiber sample input and output to a length of single mode fiber, is shown in Fig. 9(b). We obtain ~24 dB conversion at the pump wavelength, but only 0.7-2.5 dB in the 1.030-1.045 μm range where the seed is operated. This limitation can be overcome by implementing a wider bandwidth LPG [12,13], or by direct free-space excitation of the HOM [14,15]. We discuss the implications of the weaker seed conversion below.

The sample output is collimated and routed to either a power meter, optical spectrum analyzer (OSA), sampling oscilloscope, or to a Si CCD camera for mode imaging. Since the fiber is multimoded, the best way to align the input beam is by spectrally monitoring the output (as opposed to maximizing output power), since we will we get efficient PWC only when the pump and seed excite $LP_{0,1}$ at the input and are converted to $LP_{0,7}$ by the LPG. We start with only the pump on and align the steering mirrors and polarization controller at the YDFA input to maximize the spontaneous MI sidebands as monitored on the OSA. We then turn on the seed and align that beam (using steering mirrors before the beamsplitter, not shown in Fig. 9(a)) and the adjust the waveplates before the beamsplitter to maximize the converted Stokes wavelength. The measured coupling loss for either beam is typically ~0.5 dB.

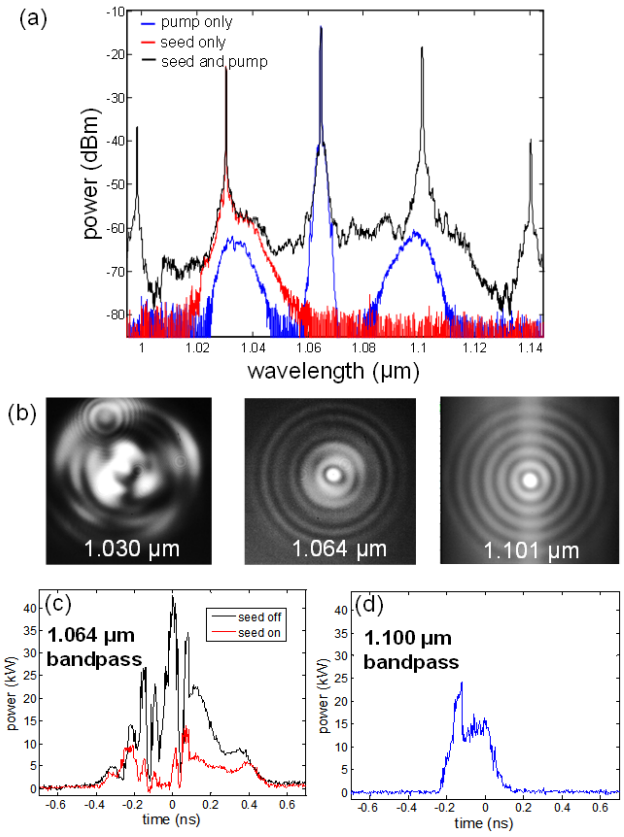

Fig. 10 (Color online) (a) Output spectrum of the PWC with the seed laser tuned to the MI peak at 1.030 μm (b) Images of the fiber output recorded at the seed (1.030 μm), pump (1.064 μm), and converted Stokes (1.101 μm) wavelengths. (c) Time traces of the output pulse filtered through a 1.064 μm bandpass filter (d) Time trace of the pulse filtered through a 1.1.00 μm bandpass filter

In Fig. 10(a) we plot representative spectra of the fiber output. As expected, we observe symmetric spontaneous MI sidebands with only the pump on (blue trace), and strong wavelength conversion to 1.101 μm when the seed laser is on and tuned to 1.03 μm, near the anti-Stokes MI peak (black trace). In Fig. 10(b), we show representative output mode images at the seed, pump, and converted Stokes wavelength. At 1.064 μm, with only the pump on, The mode looks predominantly $LP_{0,7}$-like, though the inner rings, which overlap with the core, appear measurably brighter, and with poorer extinction between rings. This is because the pronounced burnoff at the fiber center shown in Fig. 8(b) causes the $LP_{0,1}$ mode to have a non-Gaussian shape, and the inner core index step came out slightly larger than the target design, so it guides the $LP_{1,1}$ mode. Therefore, even under optimal input coupling conditions, we excite $LP_{1,1}$ to a certain degree, and after the LPG, any power not in $LP_{0,7}$ will randomly exchange between $LP_{0,1}$ and $LP_{1,1}$ over the length of the sample. At 1.030 μm, with only the seed on, the multimoded nature of the output is far more pronounced, owing to both the multimode nature of the core and the fact that the LPG mode conversion is weak (see Fig. 9(b)). Since the mode partitioning at 1.030 μm is unknown, it is difficult to estimate the how much parametric amplification is generated based on a spectral measurement alone. However, when we turn on both the seed and pump, and image the output through a bandpass filter centered near the converted Stokes wavelength at 1.101 μm, we observe a very pure $LP_{0,7}$ state, as this is the only mode for which degenerate MI-like FWM is allowed. The HOM PWC thus also provides nonlinear beam clean-up [16,17].

In Fig. 10(c) we plot the temporal profile of the sample output after spectral filtering through a 1.064 μm bandpass filter. The y-axis is scaled according to the measured average power and repetition rate. When the

seed laser is on (red curve), there is significant depletion of the of center of the pulse as compared to when the seed is off (black curve), suggesting that the power has been extracted by an ultrafast process (depletion occurs over only a few 100 ps). In Fig. 10(d) we plot the temporal profile of the wavelength converted Stokes line, filtered through the 1.100 μm bandpass. We obtain a 230 ps pulse, roughly half the width of the input pump pulse, and temporally coincident with the region of pump depletion in Fig. 10(c). This provides strong evidence that the Stokes line is created via degenerate FWM from two pump photons.

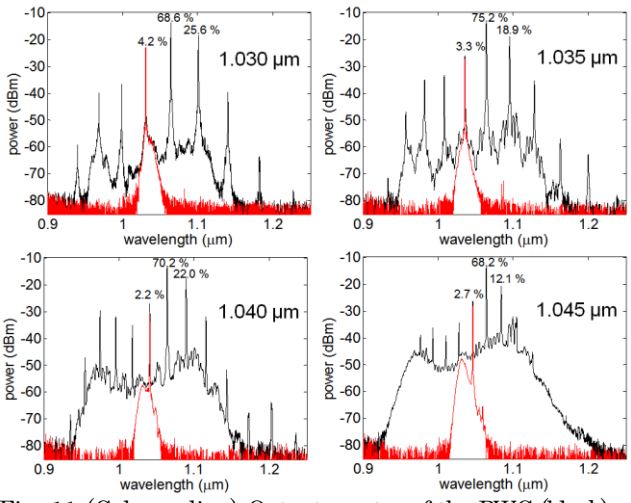

Fig. 11 (Color online) Output spectra of the PWC (black) as a function of seed wavelength. Seed laser specta are shown in red. Percentage values indicate relative power of different spectral lines.

In Fig. 11, we plot the measured spectrum as we tune the anti-Stokes seed wavelength. We obtain a maximum conversion of 25.6 % to the Stokes wavelength when the seed is tuned to 1.030 μm, closest to the MI peak. At longer wavelengths, the conversion decreases both because we are farther from the gain peak, and because the anti-Stokes seed laser spectrum exhibits stronger ASE which contributes to a more continuum-like response of the PWC, most pronounced at 1.045 μm. Since we are operating near the dispersion zero, we also observe cascade terms up to the 6th order, though together they never amount to more than 5% of the total power spectral density. Even so, we obtain 10-25% conversion from the pump and up to 71 nm wavelength translation between the anti-Stokes and Stokes lines. If we include the cascade terms, we obtain wavelength conversion over a 300 nm bandwidth.

If we compare the A_{eff} of our $LP_{0,7}$ HOM fiber to a PCF with comparable GVD for $LP_{0,1}$ at 1.064 μm [6], we have scaled A_{eff} by a factor of ~46. However, this is not to say that we have scaled the power handling by this amount. Unlike Gaussian-like modes, HOMs support discrete regions of high intensity, and it is local intensity which determines the optical breakdown threshold [9,18]. In Figs. 12(a)-(c), we plot the simulated intensity of the PCF $LP_{0,1}$ mode from [6] and the $LP_{0,7}$ used in this work, where each integrates to the same unit power. Assuming the material responses for both fibers are similar, using the HOM increases the breakdown threshold only by a factor of ~10. This means the fiber used in our experiment could handle up to ~290 kW of peak power before the onset of dielectric breakdown. But is the system scalable, even if not in a manner proportional to A_{eff}? To answer this, we simulate GVD of the $LP_{0,m}$ modes as we scale the dimensions

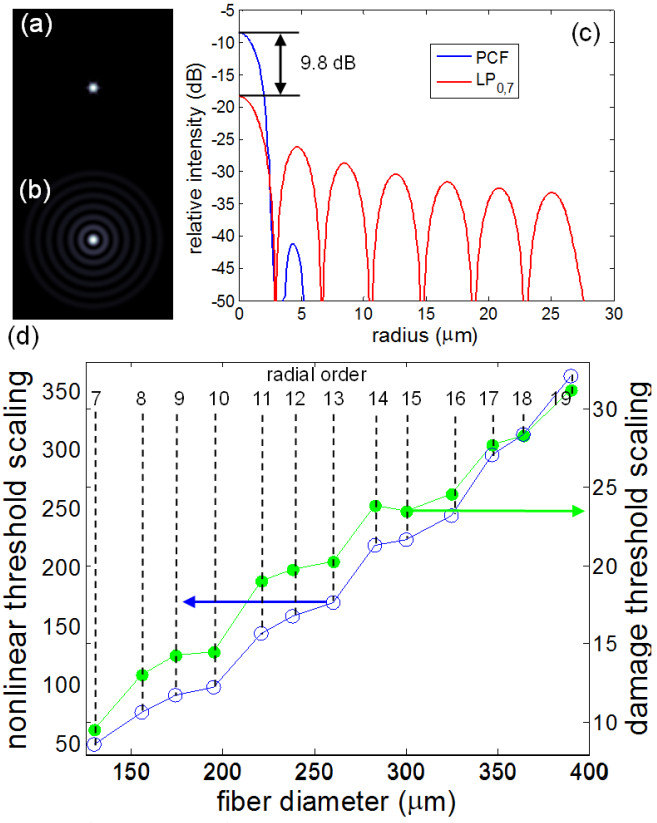

Fig. 12. (Color online)Simulated mode intensity profiles for (a) fiber $LP_{0,1}$ mode of PCF from [6] and (b) $LP_{0,7}$ mode of our HOM (c) Relative intensity of these modes (b) Power scaling of the HOM PWC relative to the PCF mode. Open circles show nonlinear scaling and closed circles show damage threshold

of the fiber and search for cases where a given mode has GVD=+5.4 ps/nm/km. These points are plotted in Fig. 12(d), where the appropriate radial orders are indicated. The left and right axes correspond to the nonlinear threshold scaling ($\propto A_{eff}$, which equivalently varies from 534 μm^2 to 5005 μm^2) and damage threshold scaling ($\propto$ local intensity, which for a 0.5 ns pulse equivalently varies from 241 kW to 994 kW peak power) relative to the PCF mode. Although damage threshold scaling grows slowly, it does monotonically increase, and from a damage threshold argument, we believe this system can be designed to handle MW-level powers.

We have demonstrated PWC at 1 μm with a 614 μm^2 mode, to our knowledge the largest area mode used to date for short wavelength parametric conversion. We measured up to 25% conversion, which can be improved by optimizing the input coupling and the fiber length. The wavelength converted pulses had up to 20 kW peak power, though with a more powerful pump, we estimate this fiber could support up to 290 kW without optical damage. This first demonstration shows that extra degrees of freedom available in multimode systems allow a far greater scope to tailor dispersion and phase-matching for parametric processes with minimal constraints on other parameters such as mode area.

- **Intermodal nonlinear optics:** The above results were dramatically enhanced by pumping much harder, enabling the creation of a supercontinuum followed by dscrete intermodal emissions all the way down to 453 nm, as illustrated in Fig. 13.

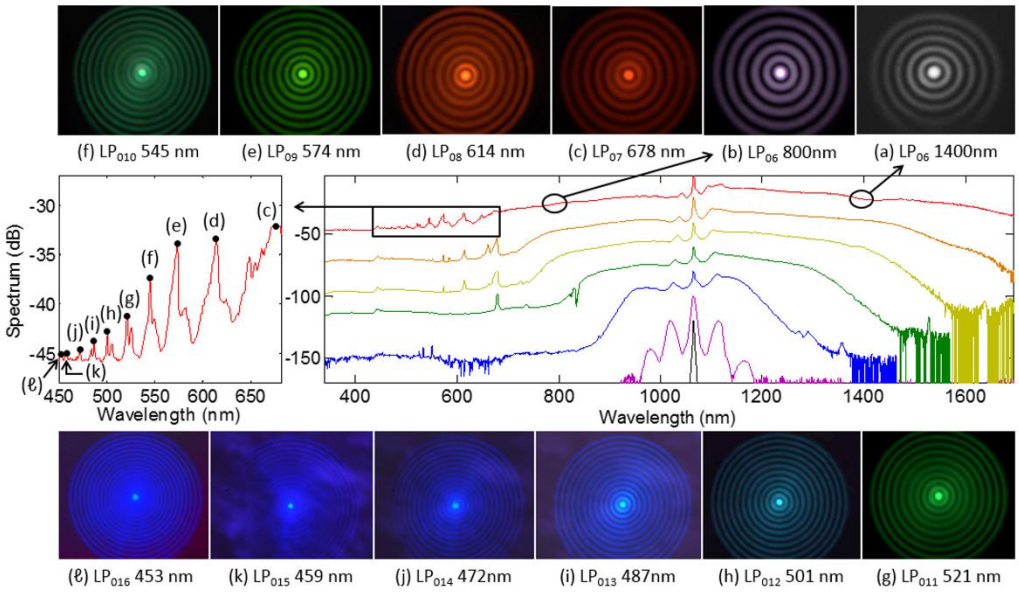

Fig. 13. Output spectra and mode images from intermodal FWM. Red, topmost spectrum was obtained with a fiber of length 16.3 m; lower spectra correspond to 10.3, 8.3, 6.3, 4.3, 2.3, and 1.3 m fiber lengths, respectively (offset for clarity), for 34.7 kW of input peak power. Detector is saturated at the pump wavelength; actual power at 1064 nm is 20 dB above that shown in the spectra. Left inset spectrum is a zoomed-in view of the 16.3 m spectrum, highlighting intermodal peaks in the visible region. Mode images (using 10-nm bandpass filters) are shown for representative portions of the continuum spectrum [(a) and (b)], and each of the discrete peaks [(c) – (ℓ)]. Between 700-1400 nm, the mode remains $LP_{0,6}$; each of the discrete peaks in the visible correspond to $LP_{0,m}$ modes of increasing radial order.

Projects/Thesis Completed with this funding:

1) MS Thesis on "C^2 Imaging for Waveguide Characterization," defended by Roman Barankov in April 2012.
2) MS project on "Tilted Fiber Bragg Gratings," awarded to Sourav Dutta in May 2011.
3) MS project on "Fiber design for optimal four-wave mixing," awarded to Yuhao Chen in May 2011

RELATED PROJECTS

A closely related project, for developing high power sources for communications, was also funded by ONR, entitled "High-Power Blue-Green Lasers for Communications." Award No. N00014-11-1-0133

PUBLICATIONS

1) L. Yan, R. Barankov, P. Steinvurzel and S. Ramachandran, "Modal-weight measurements with fiber gratings," J. Lightwave Tech., vol. 33, p. 2784, 2015.
2) J. Demas, P. Steinvurzel, B. Tai, L. Rishøj, Y. Chen, and S. Ramachandran, "Intermodal nonlinear mixing with Bessel beams in optical fiber," Optica vol. 2, p. 14, 2015.
3) J. Demas and S. Ramachandran, "Sub-second mode measurement of fibers using C2 imaging," Opt. Exp. vol. 22, p. 23043, 2014.
4) P. Steinvurzel, J. Demas, B. Tai, Y. Chen, L. Yan, and S. Ramachandran, "Broadband parametric wavelength conversion at 1 μm with large mode area fibers," Optics Letters, vol. 39, p. 743, 2014.
5) M. Laurila, R. Barankov, M. Jørgensen, T. Alkeskjold, J. Broeng, J. Lægsgaard, S. Ramachandran, "Cross-correlated imaging of single-mode photonic crystal rod fiber with distributed mode filtering," Opt. Exp. vol. 21, p 9215, 2013.
6) L. Rishøj, P.E. Steinvurzel, Y. Chen, L. Yan, J. Demas, M. Grogan, T. Ellenbogen, K. Crozier, K. Rottwitt, S. Ramachandran, "High-Energy Four-Wave Mixing, with Large-Mode-Area Higher-Order Modes in Optical Fibres," Tu.3.F.2, *European Conf. Opt. Comm. (ECOC)*, 2012.
7) J. Demas, M.D.W. Grogan, T. Alkeskjold, S. Ramachandran, "Sensing with optical vortices in photonic crystal fibers," Optics Letters, vol. 37, p. 3768, 2012.
8) Y. Chen, L. Yan, P. Steinvurzel, L. Rishoj, S. Ramachandran, "Dynamically tunable optical bottles from an optical fiber," Optics Letters, vol. 37, p. 3327, 2012.
9) R.A. Barankov, K. Wei, B. Samson and S. Ramachandran, "Resonant Bend Loss in Leakage Channel Fibers," Optics Letters, vol. 37, p. 3147, 2012.
10) D.N. Schimpf and S. Ramachandran, "Polarization-resolved imaging of an ensemble of waveguide modes," Optics Letters, vol. 37, p. 3069, 2012.
11) L.S. Rishøj, P.E. Steinvurzel, Y. Chen, L. Yan, J.D. Demas, M.D.W. Grogan, T. Ellenbogen, K. Crozier, K. Rottwitt and
S. Ramachandran, "High-Energy Four-Wave Mixing, with Large-Mode-Area Higher-Order Modes in Optical Fibres," submitted to *ECOC* 2012.
12) L. Rishøj, Y. Chen, P. Steinvurzel, K. Rottwitt, S. Ramachandran, "High-energy Fiber Lasers at Non-traditional Colours, via Intermodal Nonlinearities," CTu3M.6, CLEO, 2012.
13) Y. Chen, L. Yan, P. Steinvurzel, S. Ramachandran, "Bottle beam generated from fiber-based Bessel Beams," CLEO, 2012.
14) J. Demas, M.D. Grogan, T. Alkeskjold, S. Ramachandran, "Grating-Induced Vortices in Photonic Crystal Fiber: a pathway to ultra-high temperature sensing," JTu3K.4, CLEO, 2012.
15) R. Barankov, K. Wei, B. Samson, S. Ramachandran, "Anomalous Bend Loss in Large-Mode Area Leakage Channel Fibers," CM1N.3, CLEO, 2012.
16) D. Schimpf, F.X. Kaertner. S. Ramachandran, "Polarization-sensitive imaging of an ensemble of modes," CLEO, 2012.
17) L. Yan, R. Barankov, P. Steinvurzel, S. Ramachandran, "Side-tap modal channel monitor for mode division multiplexed (MDM) systems," OM3C.2, Optical Fiber Comm., 2012.
18) P. Steinvurzel, K. Tantiwanichapan, M. Goto, and S. Ramachandran, "Fiber-based Bessel beams with controllable diffraction-resistant distance," Optics Letters, vol. 36, p. 4671, 2011.
19) P. Steinvurzel; K. Tantiwanichapan; M. Goto; S. Ramachandran, "Diffraction control of Bessel beams generated in fiber," *Conf. Lasers & Electro-optics*, 2011.

PATENTS

1) "High-power fiber laser employing nonlinear wave mixing with higher-order modes," S. Ramachandran, US Patent 9203209.
2) S. Ramachandran, "Harsh Environment Sensors Using Gratings in Photonic Crystal Fibers," Provisional Patent Filed, then subsequently abandoned.

HONORS/AWARDS/PRIZES

(1) Top 10 downloaded Optica article in Jan. – March 2015 – (Optica 2, issue 1, 2015).

(2) Cover art article on intermodal fiber nonlinearities in Optica 2, issue 1, 2015.

(3) Top downloaded article in a month (August 2012) – Optics Letters **37** p3327 (2012).

(4) Selected for highlighting in the Virtual Journal of Biomedical Optics (VJBO) – Optics Letters **37** p3327 (2012).